Available online at www.sciencedirect.com
SCIENCE DIRECT®
Composites: Part B 34 (2003) 303–316
composites Part B: engineering
www.elsevier.com/locate/compositesb

Dynamic mode II delamination fracture of unidirectional graphite/epoxy composites

Sylvanus N. Nwosu[a,*], David Hui[b], Piyush K. Dutta[c]

[a]Department of Mechanical Engineering, University of Pittsburgh, Pittsburgh, PA 15261, USA
[b]Department of Mechanical Engineering, University of New Orleans, New Orleans, LA 70148, USA
[c]US Army Cold Region Research and Engineering Laboratory, Hanover, NH 03755, USA

Received 2 January 2002; accepted 1 April 2002

Abstract

Dynamic fracture and delamination of unidirectional graphite/epoxy composites are investigated for end-notched flexure (ENF) and center-notched flexure (CNF) pure mode II loading configurations using a modified split Hopkinson pressure bar. Results show that delamination and energy absorbed in fracture increase with impact energy with CNF > ENF. A power law analytical model reasonably describes the variation of energy release rate with delamination and energy absorbed. A crack embedded deeper in a specimen (as in CNF) contributes more to dynamic fragmentation than cracks at the surface or near the edge (as in ENF). Hackle features on mode II fracture surfaces decrease with impact energy.

Keywords: Dynamic delamination; Dynamic fracture mode; Energy absorbed; Energy release rate; Split Hopkinson pressure bar

1. Introduction

In laminated composite structures, the energy expended due to permanent plate damage is distributed among four different modes of fracture, namely: transverse matrix cracks, fiber fracture, fiber–matrix interface response, and delamination. Delamination is an interlaminar crack between plies. It has been identified as the dominant fracture mode of failure in laminated graphite systems [1,2]. Understanding dynamic delamination is important since it can lead to a catastrophic failure of the entire structure if not accounted for in the design. The increasing demand for lightweight, high strength inhomogeneous materials for military applications under dynamic conditions such as in armor/ant-armor problems, civilian applications such as in accident prevention and containment in aircraft hardening, space craft/satellite shielding from high impact velocity, and automobile industry applications such as reliability design of manufacturing processes, make the studies of dynamic fracture mechanics of utmost importance. However, the analysis of dynamic delamination is complex because of the interference of stress waves generated from the motion of the crack. Other uses include components for automotive, aerospace, marine and consumer products such as golf clubs and tennis rackets. Composites are generally used because they have desirable properties such as high strength per mass ratio, which could not be achieved by either of the constituent materials acting alone. They have unique advantages over monolithic materials, such as high strength, high stiffness, long fatigue life, low density, and adaptability to the intended function of the structure. Additional advantages include: corrosion resistance, wear resistance, appearance, temperature-dependent behavior, thermal stability, thermal insulation, thermal conductivity, and acoustic insulation. Despite their importance, dynamic fracture mechanics studies and experimental data for understanding the mode of failure and energy absorption mechanism of laminated composite plates are very limited. The call for more work in this area was recently discussed in the literature [3–6].

Research [7,8] has suggested that vertical matrix cracks near the laminate's top and bottom surfaces are due to bending stresses, while slanted matrix cracks in the laminate are the result of transverse shear stress. Delamination was attributed to pure bending and shear induced crack

* Corresponding author. Fax: +1-412-624-1108.
E-mail address: nwosu@engrng.pitt.edu (S.N. Nwosu).

1359-8368/03/$ - see front matter © 2003 Elsevier Science Ltd. All rights reserved.
PII: S1359-8368(02)00039-2

propagation. Through-the-thickness shear stresses play a dominant role in crack initiation and delamination whereas through-the-thickness normal stresses have little effect. It is generally believed that the propagation of delamination is mainly initiated by the tensile wave at interfaces and interlaminar shear through the thickness. A large stiffness mismatch (a function of the angle formed by fibers between adjacent plies) has been shown [9] to increase the potential for delamination. A stiffness mismatch is said to cause non-uniform stress distributions within the interfaces resulting in a peanut-shaped delamination. The delamination always elongates in the lowermost ply's fiber direction. It is also suggested that for a given critical degree of flexure, delamination will occur independent of the type of loading (i.e. static or dynamic) and the delamination always decreases with the decrease in angular difference between adjacent plies [9]. Results by Foos [10] show that the delamination is the dominant energy absorption mechanism in laminated composites.

Thus, modes of failure exhibited by composite material systems are complex and controlled by several energy-absorbing mechanisms operative during the process. In light of the limited body of knowledge of dynamic fracture, an investigation to document recent experimental results on the nature of dynamic delamination and energy release rate is presented in a series of two papers dealing with dynamic delamination. To give complete presentation of the experimental results, this paper deals only with dynamic mode II delamination using two loading configurations—end-notched flexure (ENF) and a new configuration referred to as center-notched flexure (CNF) and not yet reported in the literature. Basic concepts and theory of application of a modified split Hopkinson pressure bar (SHPB) is presented in some detail in Section 2 to justify its validity. Section 3 considers the experimental work on dynamic delamination and energy release rate determined from closed form equations. Part II will consider dynamic mixed mode I/II delamination.

2. Classical SHPB analysis of dynamic behavior under compression

Hopkinson [11] was the first to perform stress wave experiments using a steel bar later referred to as the Hopkinson bar. Kolsky [12] used a SHPB that consisted of a pair of long axially aligned cylindrical bars of an equal diameter for compressive tests. A test specimen was sandwiched between the bars. The impacted bar was known as the incident bar, whereas the bar opposite the specimen was called the transmitter bar. Upon generation of a uniaxial compression wave at the end of the incident bar, the wave continues down the bar's length to the bar–specimen interface. Part of the energy is reflected off the interface and is manifested as a returning tensile wave in the incident bar. Similarly, part of the energy is transmitted through the specimen into the transmitter bar and remains as a compression wave. The difference in magnitude between the transmitted and reflected waves is the energy absorbed by the specimen because of inelastic behavior. Through an analysis of the wave, the specimen's mechanical response to high strain rate compressive loading can be evaluated. The original work of Kolsky has been modified and validated for other applications [13–17].

A mechanical wave in a solid is created by a localized mechanical disturbance that propagates from one section to another. The wave characteristics depend on boundary conditions. When a propagating mechanical wave reaches a boundary that is neither free nor fixed (e.g. the boundary between two dissimilar materials, as in this investigation), a portion of the incident wave is reflected due to an impedance mismatch between the boundaries. The remainder of the wave is transmitted. For a free boundary surface, a compressive incident wave is reflected wholly as a tension wave, and vice versa. If the interaction is at a fixed boundary, a compressive or tension wave is reflected with no change in shape, phase, or intensity. In the case of a SHPB, the mechanical wave of interest is generated by a rapidly varying boundary condition caused by the impact of a striker bar on a stationary incident bar. A detailed review of wave theory is presented by others [1,18–20]. Only an outline pertinent to the present investigation is included below. Important assumptions for the mathematical description of material deformation under dynamic impact are as follows [1,21]:

1. The composite plate is elastic and its properties remain unchanged by the impact.
2. The state of the stress over the cross-sectional area is one-dimensional and uniaxial.
3. The wave is non-dispersive.
4. The state of the stress at any instant is homogenous and in equilibrium over the entire composite plate.
5. Transverse strain, lateral inertia, and body forces are all negligible.

Assumption (1) allows the use of elementary wave theory to describe wave propagation within the bars. Neglecting minor local heating of the specimen, the material properties will remain unchanged throughout the damage process. If d and L are the diameter and length of the bar, respectively, Poisson's effect is negligible when the Poisson's ratio is small compared to unity. Elementary wave theory that neglects Poisson's effect is valid for the description of wave motion in a SHPB if the wavelength (λ) of the propagating wave is 10 times the diameter (d) of the bar [21]. In the present investigation, the wavelength of the incident pulse is 610 mm compared to 25.4 mm of the rod diameter. Thus, elementary wave theory is valid.

A one-dimensional uniaxial stress condition (assumption (2)) is satisfied by making the bars prismatic and slender. Planar waves will remain planar and parallel to

the cross-section during propagation from one section to another. If L is the bar length traveled by the wave, the condition of a one-dimensional planar state of the stress is satisfied if the slenderness ratio $d/L < 1/50$ [1]. The current test apparatus has a slenderness ratio of 1/144. Thus, deviations of the wave motion from a one-dimensional planar state are negligible.

A wave is dispersive if it changes shape (through components which travel at different velocities). Issues rated to the effect of dispersion in a SHPB at a high strain rate are worthy of verification because composite materials undergo elastic deformation under dynamic or non-uniform loading conditions, making it possible for the pulse to change in amplitude and duration during transmission through the specimen. Since the calculated axial stress in the specimen depends linearly on the axial strain on the transmitter bar, wave dispersion would result in under-estimating the strength of the specimen. Assumption (3) is satisfied when the stress wave *rise time* (the time required for the stress to increase from 10 to 90% of its final value) is two or three times greater than the time required for the pulse to traverse the diameter of the rod [1]. For the current set-up, the rise time is 15 μs compared to 5 μs to traverse the diameter of the rod (three times greater). Assumption (3) is therefore satisfied.

The effect of non-uniform stress and non-equilibrium within the specimen used in this study is minimized by using longer bars and a short specimen. Since the time to traverse the specimen is short compared to the duration of the wave, equilibrium within the specimen is satisfied by the possible multiple reflections [22]. Thus, stress will be homogenous within the specimen, satisfying assumption (4). Transverse strain, lateral inertia, and body forces are all negligible since the rise time condition is satisfied and the impact is normal to the longitudinal direction. Validity of the SHPB for application to the dynamic behavior of materials is well documented [14–16].

The experimental set-up shown in Fig. 1 consists of (1) a stress generating system which is comprised of a split Hopkinson bar and the striker, (2) a special specimen fixture consisting of a specimen holder and indentor, (3) a stress measuring system made up of sensors (typically resistance strain gages), and (4) a data acquisition and analysis system. Each component of the system is described by Nwosu [23]. Dynamic loading of the composite plates is provided by a SHPB modified for perforation and fracture tests using

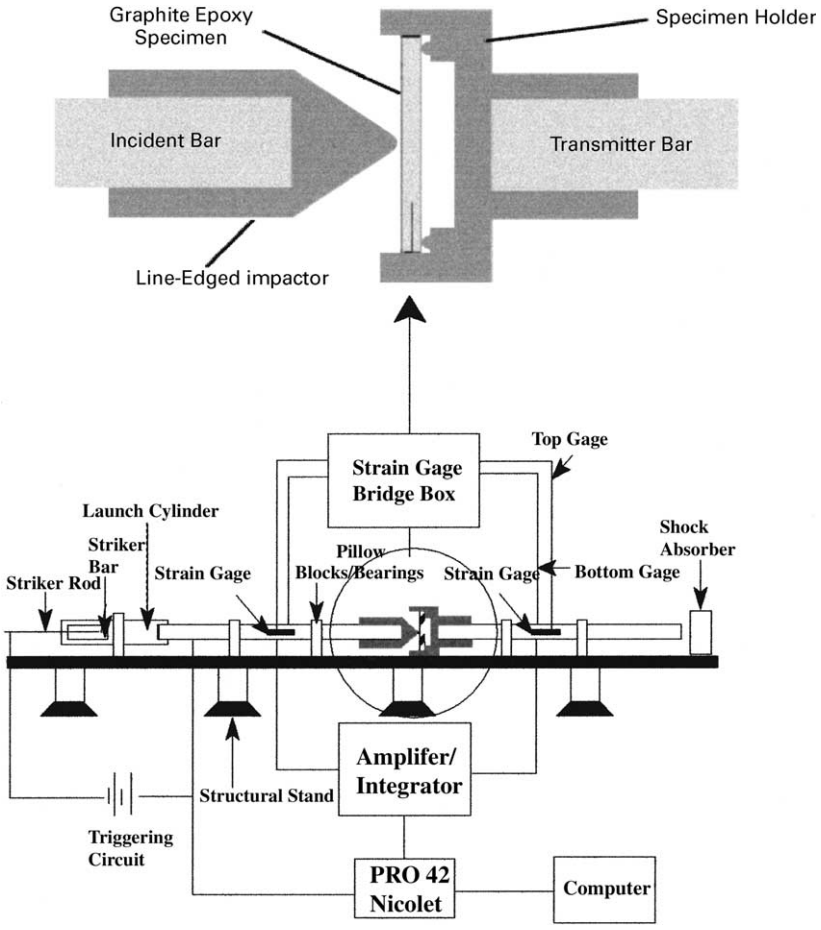

Fig. 1. Experimental set-up for dynamic mode II fracture test using ENF and CNF specimen and a fracturing split Hopkinson pressure bar.

the appropriate specimen fixture and indentor. The longitudinal impact load F_0 of the striker generates the uniaxial stress pulse transmitted to the incident bar as

$$\sigma(t) = \frac{F_0}{A} = (\rho c_0) V_p(t) \tag{1}$$

where $c_0 = dx/dt$ is the velocity of the wave pulse, $V_p(t)$ is the particle velocity, and ρ is the density of the striker material. Accurate measurements of the wave pulse and particle velocity in dynamic impact studies are important since the wave pulse is really the propagation of the disturbance or vibration of the particles. The amplitude of the incident wave pulse depends on the impact velocity (a function of the applied air pressure) and material properties of the striker. The measurement is expected to be accurate when measured at steady state conditions. Theoretically, such a steady (equilibrium) condition is satisfied by the continuity condition. The particle displacement is expressed as:

$$u(t) = \int_0^t V_p(t)dt = \frac{c_0}{E_0}\int_0^t \sigma(t)dt \tag{2}$$

Upon the arrival of a compressive incident wave at the specimen/incident bar interface, the wave is partially reflected (because of the impedance mismatch) and partially transmitted through the specimen. Thus, the net displacement at the surface is given as

$$U_1(t) = u_i - u_r = \frac{c_0}{E_0}\int_0^t [\sigma_i(t) - \sigma_r(t)] \tag{3}$$

where $c_0 = (E_0/\rho)^{1/2}$ and E_0 are the bar wave velocity and Young modulus, respectively, and σ_i and σ_r are the incident and reflected stress pulses, respectively. Similarly the net displacement at the specimen–transmitter bar interface is expressed as:

$$U_2(t) = u_t(t) = \frac{c_0}{E_0}\int_0^t \sigma_t(t)dt \tag{4}$$

Thus, from Eqs. (3) and (4), the net displacement in the sample is given as:

$$U_1(t) - U_2(t) = u_n(t) = \frac{c_0}{E_0}\int_0^t [\sigma_i(t) - \sigma_r(r) - \sigma_t(t)]dt \tag{5}$$

Eq. (5) represents the specimen displacement due to the interaction of compressive and tensile waves in the sample. The specimen's strain ($\varepsilon_s(t) = u_n(t)/L_e$) and strain rate for bars of the same cross-sectional area can be expressed, respectively, as

$$\varepsilon_s(t) = \frac{c_0}{L_e}\int_0^t (\varepsilon_i(t) - \varepsilon_r(t) - \varepsilon_t(t))dt \tag{6}$$

and

$$\frac{\partial \varepsilon_s(t)}{\partial t} = \frac{c_0}{L_e}(\varepsilon_i(t) - \varepsilon_r(t) - \varepsilon_t(t)) \tag{7}$$

since $\sigma(t) = E_0\varepsilon(t)$.

2.1. Stress, particle velocity and force measurements

The particles in the incident bar will propagate to the right at a relative velocity of V_b in the longitudinal direction of the wave pulse. With a specimen of cross-sectional area, A_s, sandwiched between the incident and transmitter bars of the cross-section area, A_b, equilibrium at the interfaces is satisfied by the continuities of forces and velocities at the interfaces such that the particle velocities, sample stress, strain and strain rate for a thin sample are easily derived as [23]:

$$V_s = \frac{c_0}{E_0}(\sigma_i - \sigma_r) \tag{8}$$

$$\sigma_s(t) = \frac{A_b}{A_s}E_0\varepsilon(t) \tag{9}$$

Assuming equilibrium in short specimen, $\varepsilon_t = \varepsilon_i + \varepsilon_r$, and Eqs. (6) and (7) give the strain and strain rate as:

$$\varepsilon_s(t) \approx \frac{-2c_0}{L_e}\int_0^t \varepsilon_r(t)dt \qquad \varepsilon_s(t) \approx \frac{-2c_0}{L_e}\varepsilon_r(t) \tag{10}$$

2.2. Energy measurements

The net energy produced by the indentor and carried by the propagating compressive wave to the composite plate is given by

$$E_p = \int_0^t F_i(t)du_n \tag{11}$$

where $F_i(t) = A(\sigma_i(t) - \sigma_r(t))$ is the net compressive loading force and du_n is the net plate displacement given by Eq. (5), and can be obtained as the integrated area of the force–displacement curve over the wave's duration. Damage to the laminate occurs by the transfer of energy given by Eq. (11) during the damage process. Substituting Eq. (5) into Eq. (11), and neglecting energy losses within the fixture, the total energy absorbed for the damage process for the plate is given as $E_A = E_i - E_r - E_t$ and expressed as

$$E_A = \left(\frac{Ac_0}{E_0}\right)\int_0^t [\sigma_i(t)^2 - \sigma_r(t)^2 - \sigma_t(t)^2]dt \tag{12}$$

where $E = (Ac_0/E_0)\int \sigma^2\, dt$ has been written for incident (E_i), reflected (E_r) and transmitted (E_t) energies. The numerical integration is carried out with all time shifted to zero and all three waves beginning at the same time and for the same time duration, t.

Experimental parameters for AS4/3501-6 toughened epoxy unidirectional $[0]_n$ composites used by Reeder [24] and Reeder et al. [25] are 131, 9.7, and 5.9 GPa for the longitudinal modulus (E_{11}), transverse modulus (E_{22}), and shear modulus (G_{13}), respectively. The dimensions of the graphite/epoxy specimens used in this present study are 52 mm in total span ($2L$), 25.4 mm in width (B), and

0.27 mm/ply in thickness ($2h$). Dimensions were chosen to be of the same ($2L/b$) scale with Reeder et al. [25]. P_m, is the stress wave loading force, determined as the peak loading force in the force–displacement curve and is related to the stress field at the crack tip. This force is stress wave dependent, and is the driving force for damage propagation. The delamination length, a, is determined by measuring the length of the mid-thickness crack along the specimen's edge. A microscope is used for clearer viewing of the extent of the delamination. When the specimen was pulled apart through the middle, it was observed that the length of the delamination zone measured from the edge to the crack tip was a little longer than the edge crack length due to the effects of deflection and curvature. In cases where the specimen is completely split through in mid-thickness by the loading force, the delamination length is taken as the total specimen span ($2L$).

2.3. Dynamic delamination

The onset of delamination has been determined by application of acoustic emission [26] piezoelectric sensors [27,28] and other vibration-based methods [29]. Dynamic delamination propagation in composite materials is made possible by the energy flow into the crack tip. This energy flow is physically defined by the energy release rate and has been fundamental to characterizing the dynamic fracture process and determining the effect of delamination on the structural strength of the composite panel [30]. These researchers reported that embedded delamination create imperfection that can trigger dynamic crack propagation of the delamination in the presence of compressive loading. Tsai et al. [31] used a modified ENF specimen and MTS and determined that the dynamic mode II dominated delamination and energy release to be same as in the static case. However, this conclusion requires further investigation since the use of the MTS system to approximate a purely dynamic event could not be a conclusive generation. MTS is a static or quasi-testing machine and ignores the stress field at the crack trip that is responsible for dynamic crack propagation.

In their analysis of interlaminar fracture in uniaxial fiber–polymer composites based on beam theory analysis, Hashemi et al. [32] and Williams [33] developed a general closed form equation for interlaminar energy release rate G based on bending moments applied to lower and upper sections of a laminated composite plate. Generally, the energy release rate is related to the resistance of materials to delamination-related failure. A general quasi-static expression for the energy release rate was given as

$$G = \frac{3}{4B^2h^3E_{11}}\left(\frac{M_1^2}{\xi^2} + \frac{M_2^2}{(1-\xi)^2} - (M_1+M_2)^2\right) \tag{13}$$

where h is half of the plate thickness, $\xi = h_1/2h$, and E_{11} is the axial modulus of the laminate, M_1 and M_2 are the moments of the lower and upper sections of the laminated plate about the crack tip, B is the total width of the plate, h_1 and h_2 are the thickness of the upper and lower sections, respectively, and mode I and mode II energy release rates are given as:

$$G_I = \frac{6h_1^3}{B^2h_2^3(h_1^3+h_2^3)E_{11}}\left(M_2 - \frac{h_2^2}{h_1^2}M_1\right)^2 \tag{14}$$

$$G_{II} = \frac{18h_1h_2}{B^2(h_1+h_2)^2(h_1^3+h_2^3)E_{11}}(M_1+M_2)^2 \tag{15}$$

Eqs. (14) and (15) also predict the presence of mode I in any loading condition in which h_1 is not equal to h_2. This paper considers only the case of pure mode fracture. However, as noted by Reeder et al. [24,25] and O'Brien and Martin [34], even in cases where pure mode II is certain to be the dominating mechanism, a small fraction of mixed mode effect could be expressed.

2.3.1. Pure mode II end-notched flexure testing

ENF test is usually used for the pure mode II test with the specimen loaded at the center, and simply supported near both ends. The ENF specimen for this investigation is shown in Fig. 2. The specimen is fabricated with 0.13 μm Teflon pre-crack placed at mid-thickness from one edge. Mode II fracture is expected to be maximum when the loading is at the center because of the maximum bending effect. Based on Eq. (15), the energy released rate for this specimen is estimated by the closed form equation expressed as

$$G_{II} = \frac{9}{16}\left(\frac{P_m^2}{B^2h^3E_{11}}\right)(a+\chi h)^2 \tag{16}$$

where χ is a correction for some deflection, curvature effect, and rotation at the crack tip, and given as

$$\chi = \left[\frac{E_{11}}{11G_{12}}\left(3 - 2\left(\frac{\Gamma}{1+\Gamma}\right)^2\right)\right]^{1/2}$$
$$\Gamma = \frac{1.18\sqrt{E_{11}E_{22}}}{G_{12}} \tag{17}$$

P_c is the critical load (the maximum load just before unloading of the crack front) at the load–displacement curve and delamination length, a, is determined by measuring the length of delamination or interface crack length. Moderate impact energy is needed to initiate the crack in the ENF specimen. At certain high strain rates, the crack propagates through the specimen, splitting it to the end (crack run-off).

2.3.2. Center-notch flexure testing

The proposed CNF specimen configuration is similar to ENF pure mode II fracture but with a 0.13 μm Teflon insert in the center mid-thickness located between the two middle

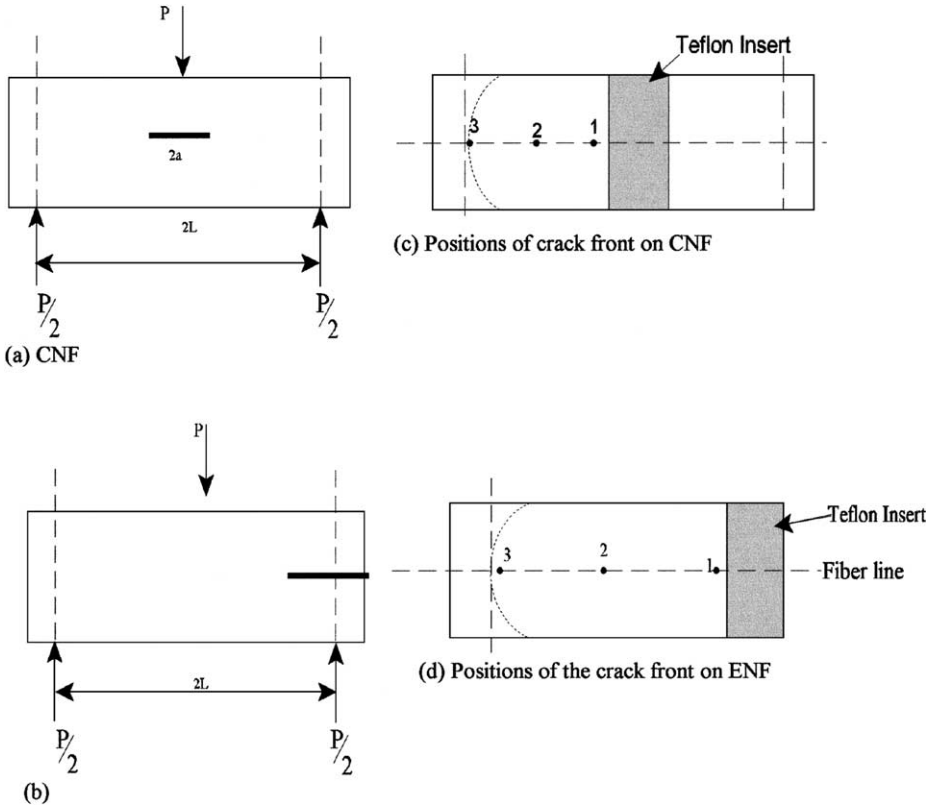

Fig. 2. Symmetrical loading and positions of the crack tip on the fracture surface for end-notch flexure (ENF specimen) and center-notch flexure testing (CNF specimen) for pure mode II fracture testing.

plies as shown in Fig. 2. A line edge loading applied at the center creates a bending at the center with respect to the support at both sides of the specimen. Pure mode II is expected to dominate the fracture toughness with $D = 0$ since in-plane opening due to tension is negligible. Therefore $G_I = 0$, and G_{II} is given by Eq. (18) after replacing a in Eq. (16) by $a/2$.

$$G_{II} = \frac{9}{16}\left(\frac{P_m^2}{B^2h^3E_{11}}\right)\left(\frac{a}{2} + \chi h\right)^2 \tag{18}$$

From Eqs. (16) and (18), energy release rate is proportional to the second power of delamination and loading force. It should be noted that these are quasi-static equations used here only as an approximation. For complete dynamic test analysis, kinetic energy and rate effects must be considered for the total strain energy. Under dynamic loading conditions in which the crack is propagating at a certain speed, determination of stress intensity factors or energy release rates is very complex because the crack is mainly loaded by the stress wave. The interlaminar fracture toughness is therefore expected to depend mainly on the state of the stress around the crack front. Tensile pulse propagating through the material is mainly responsible for the crack propagation, and is reflected at the surface. The resulting flexure vibration usually makes the analysis difficult. For this investigation, flexure vibration is assumed minimal when only the first full wave to arrive at the specimen surface is used for the analysis. The experimental dynamic delamination data will be used to estimate the energy release rate using the quasi-static equations presented here. By attaining a quasi-static state of stress in the vicinity of the crack tip, dynamic fracture toughness has been successfully evaluated by others [35,36] using quasi-static and static formulations. The present work differs from previous work in that the time-dependent loading force in our formulation is due to the stress field, which is responsible for the propagation of the crack tip. Analysis in the present investigation will indicate whether the proposed center-notched loading configurations can simulate pure mode fracture behavior better than the conventional ENF.

3. Experimentation

Fig. 1 shows the modified SHPB. The modified SHPB apparatus consists of incident, transmitter, and striker bars (300 maraging AMS 6414 steel), each being 25.4 mm (1 in.) in diameter. The incident and transmitter bars are 3.66 m (12 ft) in length, while the striker bar is 0.305 m (1 ft) long. The striker is housed inside a 0.610 m (2 ft) launch cylinder and is driven by compressed air of up to 1.72 MPa (250 psi). The compressed air reservoir is of high volume so that

the desired pressure is effectively maintained throughout the launch event. To begin each test, the desired pressure is manually set using a gauge between the launch cylinder and the reservoir. A switch in the control room activates the opening of a quick-acting solenoid valve, allowing compressed air acceleration of the striker into the incident bar. The impact-end of the striker is spherically rounded with a 0.0508 m (2 in.) radius for a repeatable point of contact with the incident bar on a plane centrally normal to the longitudinal direction of the wave propagation. Proper axial alignment between the striker and incident bars is ensured to minimize flexure. Uniaxial waveform generated in the bar determines the rate at which energy is transferred from the bar to the laminated plate. The shape of the waveform is controlled by the geometrical shape of the striker and the impact velocity. The stress wave amplitude varies with impact velocity, while the stress profile changes with striker geometry [37]. Incident and transmitter bars are guided through pillow blocks containing low-friction ball bearings. The bushings (mounted on a rigid steel channel which is backed-up by an I-beam) support the bar shifts without restraining them. The support can be adjusted laterally and vertically for proper alignment. To minimize vibration, the unit is anchored to steel beams running through a 102 mm (4 in.) steel-reinforced concrete deck. A 6.35 mm (0.25 in.) diameter rod is attached to one end of the striker and protrudes outside the cylinder as a means of adjusting the stroke length (and therefore striker velocity). Venting holes along the launch tube maintain a low pressure zone in front of the striker and prevent the possibility of multiple impacts.

Experimental parameters for AS4/3501-6 toughened epoxy composites used by Reeder [24] and Reeder et al. [25] are 131, 9.7, and 5.9 GPa for the longitudinal modulus (E_{11}), transverse modulus (E_{22}), and shear modulus (G_{12}), respectively. The dimensions of the graphite/epoxy specimens used in this present study are 52 mm in total span ($2L$), 25.4 mm in width (B), and 0.27 mm/ply in thickness ($2h$). Dimensions were chosen to be of the same ($2L/B$) scale as in Ref. [24]. P_c, is the stress wave loading force, determined as the peak contact force in the force–displacement curve and is related to the stress field at the crack tip. This force is stress wave dependent, and is the driving force for the propagation of the stress field. Such stress has been shown not to be simply related to any externally applied force when the loading exceeded a certain value [34]. The delamination length, a, is determined by measuring the length of the mid-thickness crack along the specimen's edge. A microscope is used for clearer viewing of the extent of the delamination. When the specimen was pulled apart through the middle, it was observed that the length of the delamination zone measured from the edge to the crack tip was a little longer than the edge crack length due to the effects of deflection and curvature. In cases where the specimen is completely split through in mid-thickness by the loading force, the delamination length is taken as the total specimen span ($2L$).

4. Experimental results and discussions

4.1. Characteristics stress waveform

The stress waveforms for the different failure modes and loading configurations are shown in Fig. 3. For pure mode II (CNF) configuration, the waveform shows greater stress wave distortion after the first reflection and smaller transmission of the incident wave than the ENF specimen. This observation indicates that the ENF specimen experiences greater loading of the stress wave than the CNF. As evidenced in Fig. 4, the ENF specimen sustains higher strain rate and higher loading force than the CNF specimen. The reflected wave is the major contributor the force–time history and is mainly affected by surface conditions.

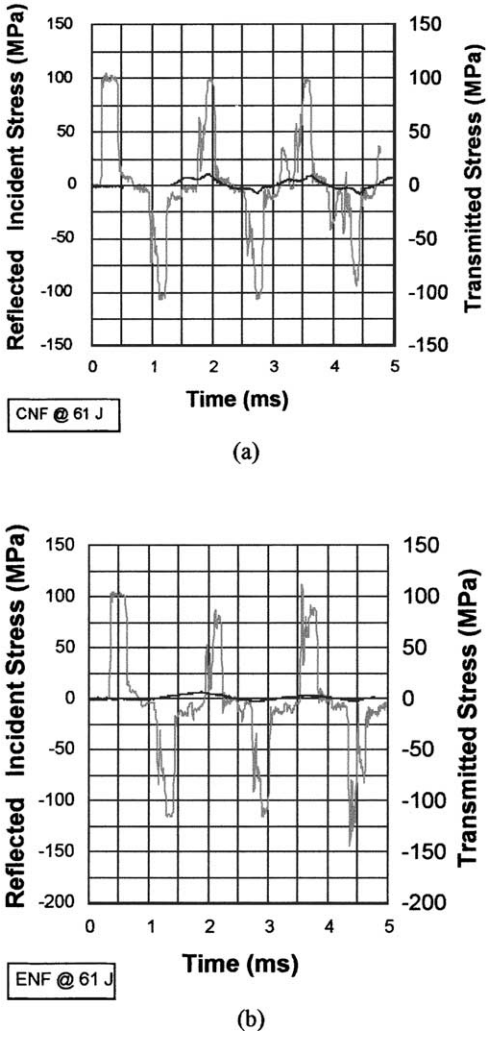

Fig. 3. Stress waveforms for pure mode II using 24-ply (a) CNF specimen and (b) ENF specimen.

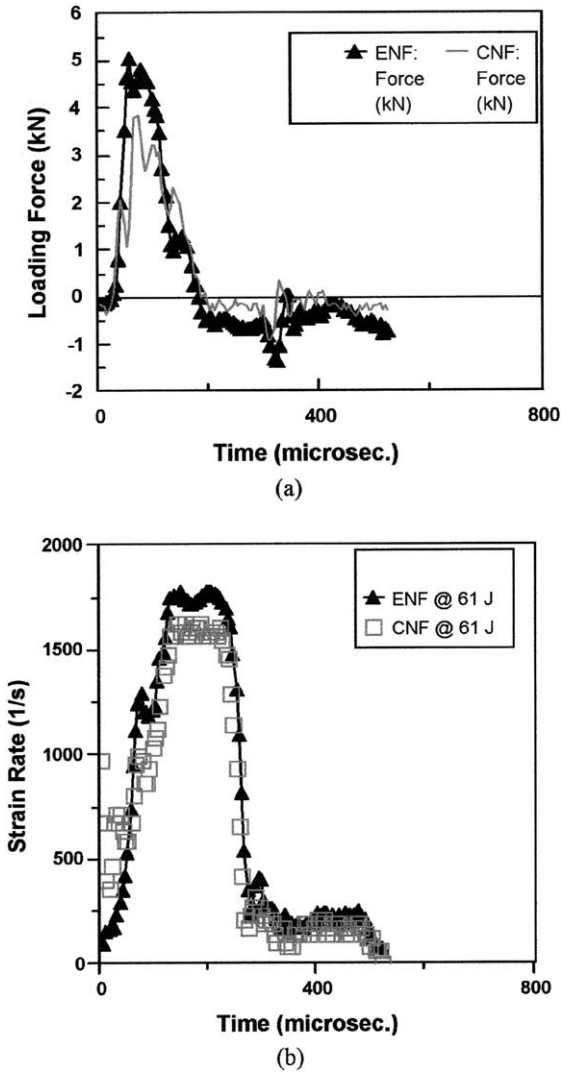

Fig. 4. Time histories of (a) loading force (b) strain rate for 24-ply ENF and CNF specimen generated at 61 J impact energy.

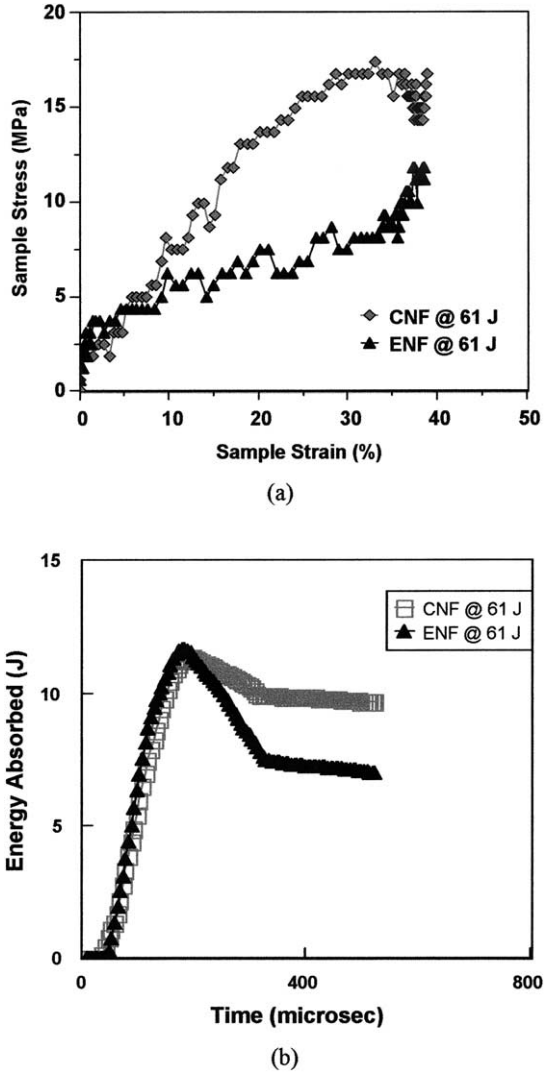

Fig. 5. Dynamic sample response (a) sample stress (b) energy absorbed for 24-ply ENF and CNF specimens at 61 J impact energy.

The force–time history shows a greater tensile release wave in the ENF than the CNF configuration. Since the crack propagation in the CNF specimen is constrained to initiate from the center, it was hypothesized that the greater tensile release wave for the ENF is due to the greater flexing and crack instability in ENF than CNF. Thus, the energy absorption history and stress–strain curves in Fig. 5 for ENF and CNF loading configurations clearly shows that at the same energy of 61 J, the CNF specimen exhibits a higher compressive strength and sustains higher energy absorption than the ENF. This implies that a crack near the surface or edge of a structure will have a greater tendency to reduce the strength of the materials to failure than when embedded deeper in the structure. The results clearly show that for approximately the same loading force, more energy is absorbed in mode II with a higher tensile release wave amplitude than the mixed mode I/II [38]. This is a consequence of the confinement of the wave described earlier.

4.2. Variation of relative delamination with impact energy

The variation of relative delamination, and delamination in Figs. 6 and 7, respectively, show that delamination increases with impact energy. Some energy is expended in the early stage to overcome friction and initiate the crack propagation, and more energy is absorbed to sustain the crack propagation. For the ENF specimen, the delamination was constant initially for impact energy above 5.0 J. Beyond the threshold impact energy, and as more energy is pumped into the crack tip, relative delamination increases with impact energy until the span of the specimen is reached at about 67 and 75 J for the 16- and 24-ply specimen, respectively. In the case of pure mode II CNF, no delamination was observed until a minimum energy of 46 J was reached after which the delamination remained constant before decreasing as fragmentation dominated the failure mechanism [38,39]. Thus, the threshold energy at which the crack propagates through the entire span is higher

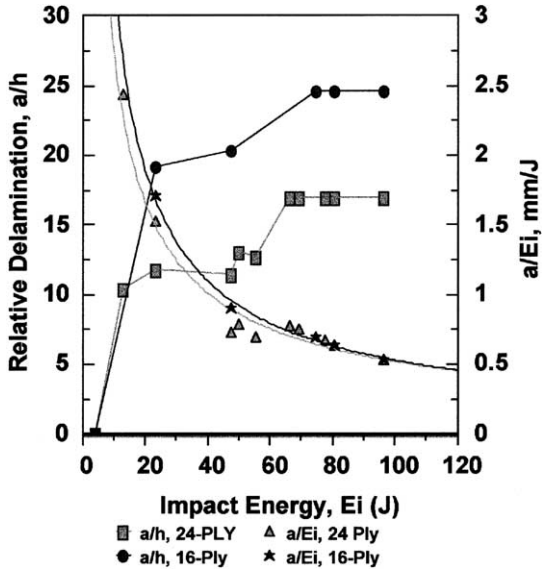

Fig. 6. Variation of thickness and energy normalized delamination with impact energy for ENF 16- and 24-ply specimens.

for ENF than CNF because of increased fragmentation at a lower energy for the CNF specimen. At $E = 23.6$ J, a/h are 11.4 and 19.2 for the 24- and 16-plies, respectively, compared to 16.5 and 24.7 at 80.5 J showing that for the same impact energy delamination is thickness dependent. However, the ratio of change of delamination (Δa) to sample thickness (Δx) remains approximately constant and independent of energy. These two results show that change in delamination is proportional to change in impact energy. The ratio of delamination to impact energy decrease non-linearly as

$$\left(\frac{a}{E_i}\right)_x = D_E E_i^n \tag{19}$$

Where D_E and n are 14.7, -0.724 ($r^2 = 0.949$) for the 24-ply specimen and 20.7 and -0.795 ($r^2 = 0.992$) for the 16-ply specimen in Fig. 6. The result shows that the ratio of delamination to impact energy is maximum at lower energy and approaches a constant value independent of thickness as impact energy approaches 67 J or the crack propagates to the span of the specimen. Thus, the ratio of change of delamination to change in impact energy remains constant independent of sample thickness.

4.3. Fragmentation

In more than 90% of the cases, it was observed that the CNF specimen mainly fragmented before any visible side crack as shown in Fig. 7. The residual energy is reflected back into the specimen resulting in increased fragmentation. However, the results reasonably reveal that when the initial crack is within the specimen mid-center as in the CNF specimen, the major failure mechanism is delamination and fiber breakage at low energy and fragmentation at higher energy. Fragmentation results from dynamic crack

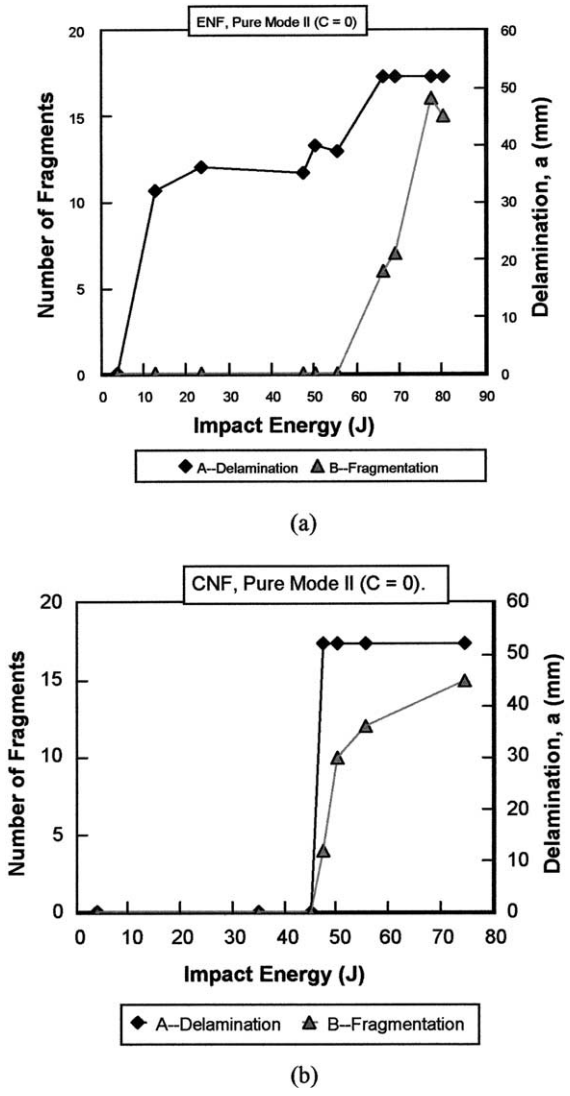

Fig. 7. Effect of impact energy on fragmentation for 24-ply (a) ENF and (b) CNF specimens.

propagation, and is the dominant mode of fracture in the CNF specimen, and in both ENF and CNF at high impact energy. This fragmentation is due to continued branching of the crack. Previous investigators have shown that fragmentation occurs when the stress waves reflected from the specimen boundaries return to the crack tip [30]. We infer from the results that crack initiation, fracturing, and crack propagation (leading to splitting or fragmentation) are seen as three distinct failure regions for the specimen.

4.4. Variation of G_{II} with delamination, energy absorbed, and impact loading energy

Figs. 8 and 9 display the variation of energy release rate with delamination, energy absorbed, and impact energy. The G values are determined from the closed form models developed in earlier sections. The energy release rate is not a linear function of energy absorbed. The experimental data

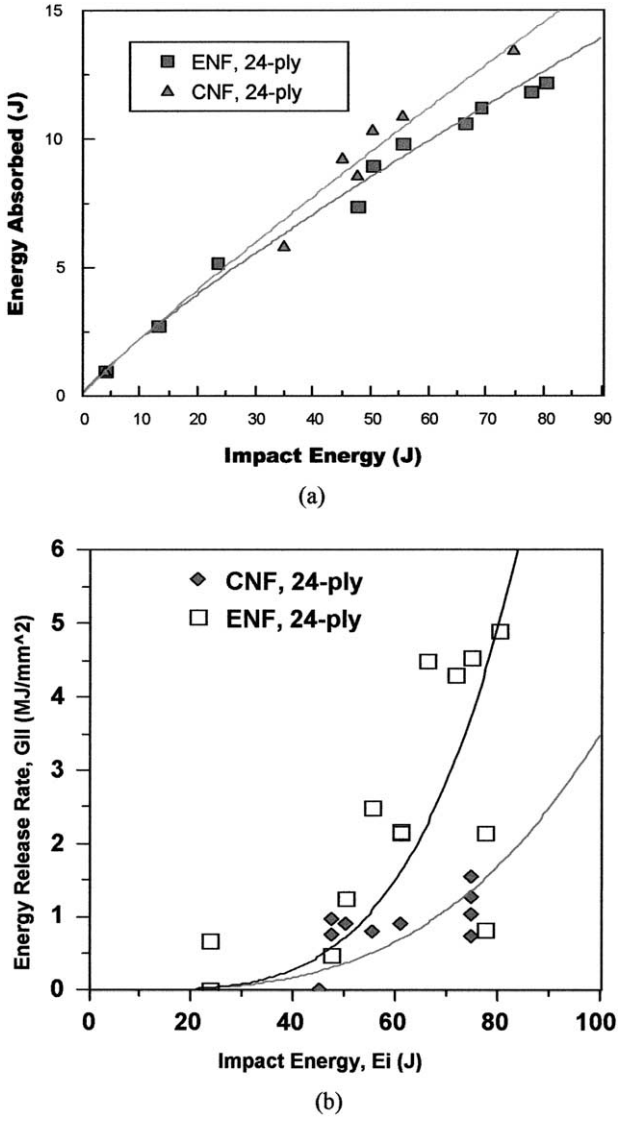

Fig. 8. Effect of impact energy on (a) energy absorbed and (b) energy release rate. Solid curves are power law fit to experimental data.

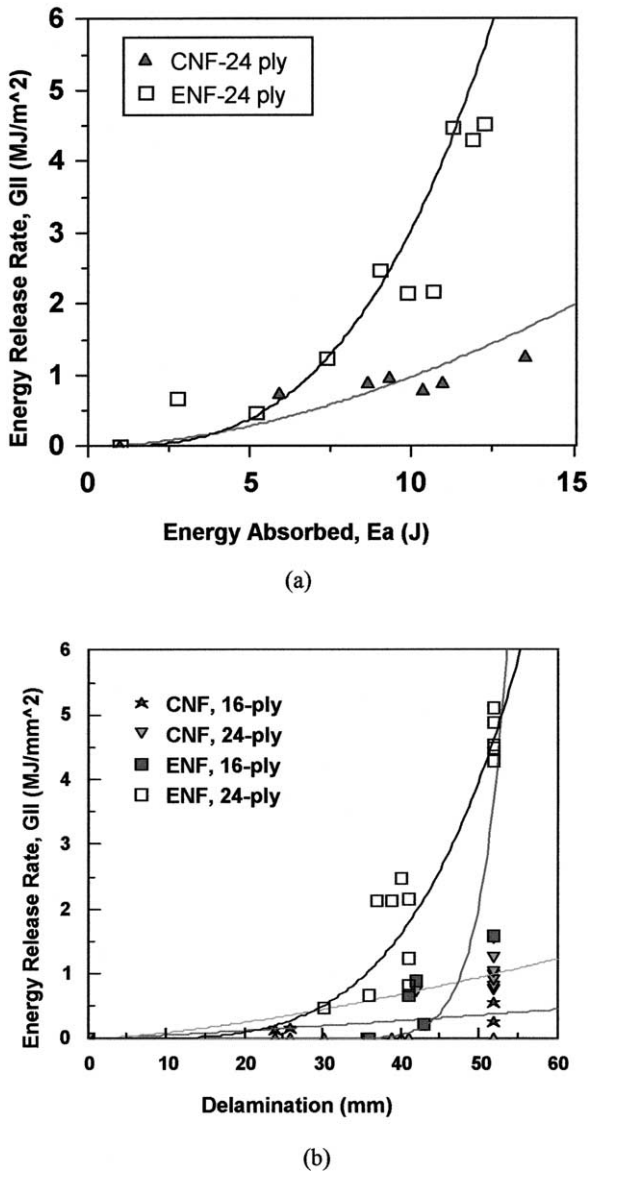

Fig. 9. The effect of (a) energy absorbed and (b) crack delamination crack growth on energy. Solid curves are power law fit to the experimental data.

were fitted to a power law model expressed as

$$G_{II}(X) = \beta_{II} X^{\eta} \tag{20}$$

where the variable X represents energy absorbed (E_A), impact energy (E_i) or delamination (a_0), the parameters β_{II} and η are determined for each variable. Table 1 shows that ENF has higher exponent n and lower β_I values than the CNF specimen. With η-values of 1.5 and 4.0 for CNF and ENF, respectively, the fitting curves show that the fracture behavior using CNF loading configuration is more predictable of conventional mode II Eq. (18) than for ENF. The energy release rate using CNF is proportional to 1.5 power of delamination and 1.8 for energy absorbed. Since energy absorbed is proportional to the second power of the stress amplitude (and since $\sigma(t) = F(t)/A$), the energy release rate is expected to be proportional to a second power of energy absorbed or loading force as in Eq. (7).

Table 1
Analytical model for variation of energy release rate with delamination, energy absorbed and impact energy

	n	K_{II}
$G_{II}(a) = K_{II} a^n$		
ENF	4.0	0.535
CNF	1.5	3260
$G_{II}(E_a) = K_{II} E_a^n$		
ENF	3.0	3160
CNF	1.8	17,100
$G_{II}(E_i) = K_{II} E_i^n$		
ENF	4.1	0.067
CNF	3.3	0.973

4.5. Effect of loading energy on ENF and CNF fracture surface morphology

Fig. 10 shows typical SEM photographs for single ENF and CNF mode taken at the region near the initial crack insert (assumed close to the crack tip). For low loading energy of 48 J for the CNF, fibers are seen exposed with irregularly spaced poorly defined medium-coarse to fine hackle marks. In some cases, the fibers are almost completely resin covered with wider hackle marks interspersed with areas of finer hackles. Very coarse hackles and cracks perpendicular to the fibers can be seen with some fracturing in the lower middle of the picture. More fibers are exposed per unit area with minor matrix debris visible. As loading energy is increased to 61, more fibers are exposed around the insert end with some incipient hackle marks at irregular spacing. Compared to the CNF specimen, the SEM photographs of ENF surfaces near the insert end at 48 J show wider hackle marks bending to the right with evidence of some resin debris removed, fiber pull-out, and breakage. Some fine, regularly spaced hackles could clearly be seen. As the loading energy is increased to intermediate of 61 J, less regularly spaced medium coarse to fine hackles are seen, and with some evidence of fiber pull-out and fiber breakage. At higher loading energy of 75 J, the fibers are extensively exposed; some desegregation of the fibers is visible.

Definite characterization of the failure mode based on the above qualitative analysis is generally difficult because the fracture surfaces usually exhibit a convolution of multi-mode features that often makes isolation difficult. In the present investigation, a qualitative analysis of the surface was done by counting the actual exposed fibers, hackle marks along each fiber, and by measuring the span of

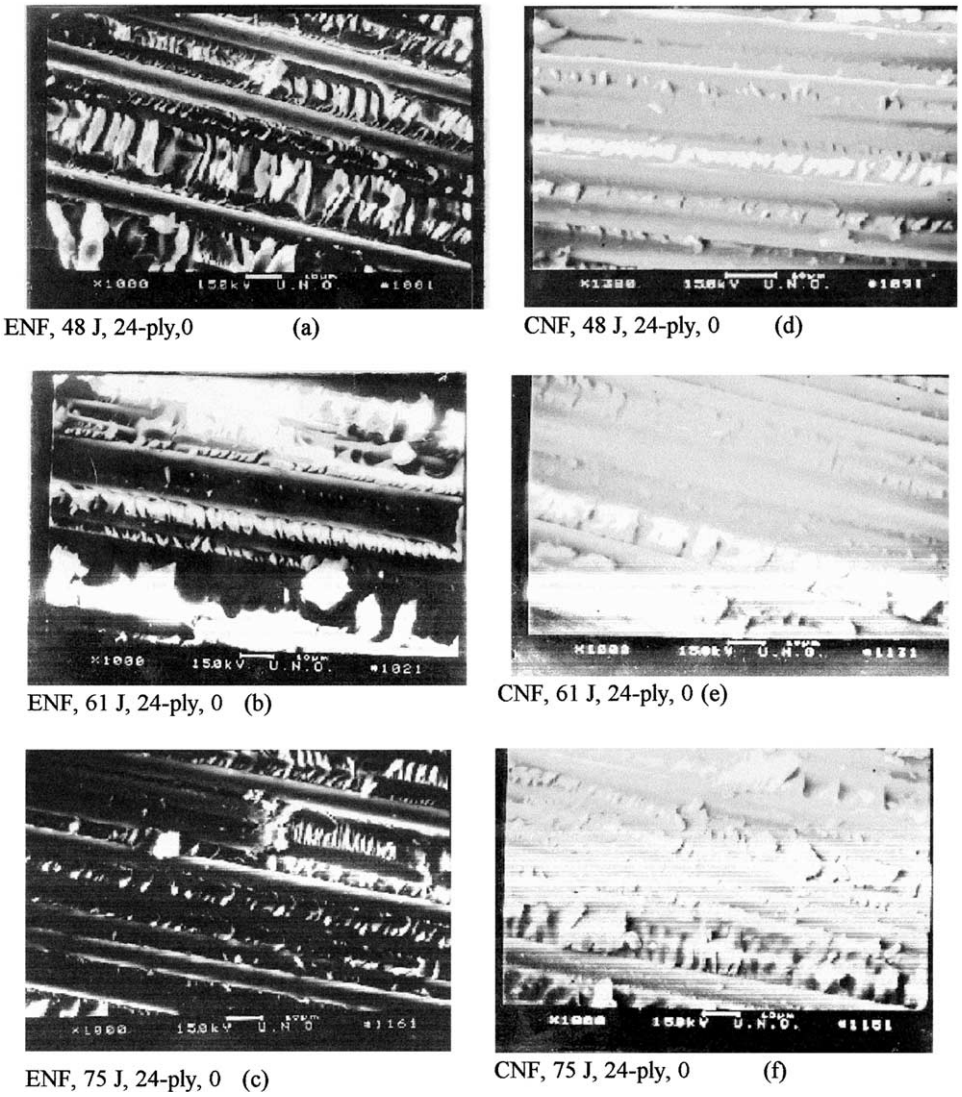

Fig. 10. SEM photographs of 24-ply for (a–c) ENF surfaces and (d–f) CNF surfaces near the end of insert at varying impact energy loaded at the center.

the fiber. The distribution has been referred to as the 'DNA' of hackle marks formation where the averaging of the hackles de-convolutes the interacting modes into the average dominating mode of failure [39]. Greater frequency of well-developed hackles is an indication of the high energy absorption presence of interlaminar shear forces and (pure mode II) shearing fracture mode. A lower frequency of coarse hackles or increased fine or incipient hackles indicate smooth surfaces, weak interfacial bonding, and absence of interlaminar shear forces (pure mode I fracture). The distribution clearly shows that hackle formations decrease as the loading energy increases, with maximum hackles occurring at intermediate energy than decreasing at high energy. For the 24-ply ENF and CNF specimens, maximum density occurs at an impact energy of 61 J. Thus, the hackle density starts to decrease as the delamination length approaches the span of the specimen or as the energy approaches the critical energy for unstable delamination.

Figs. 11 and 12 show a quantitative summary of the results where the hackle counts of all sizes on the entire fractured surface are plotted against the impact energy or position of the crack. The plot shows that a 24-ply ENF specimen has a higher marks density than the 24-ply CNF specimen at the same energy. More pure mode II feature are developed at positions between the center and the edge of the specimen because the crack tip velocity is expected to be most stable at that region provided that the energy is low. For both ENF and CNF, the total hackle marks density reached a maximum when the crack tip is between the insert end and the edge of the specimen and decreases as the crack tip approaches the edge of the specimen. In all cases, it is evident that CNF loading exhibits better developed hackles and pure mode II features than ENF. Since hackle feature indicate presence of shear stress or mode II feature, these results show that a crack embedded deeper in a specimen as in CNF contributes more to mode II fracture than cracks at the surface or near the edge as in ENF.

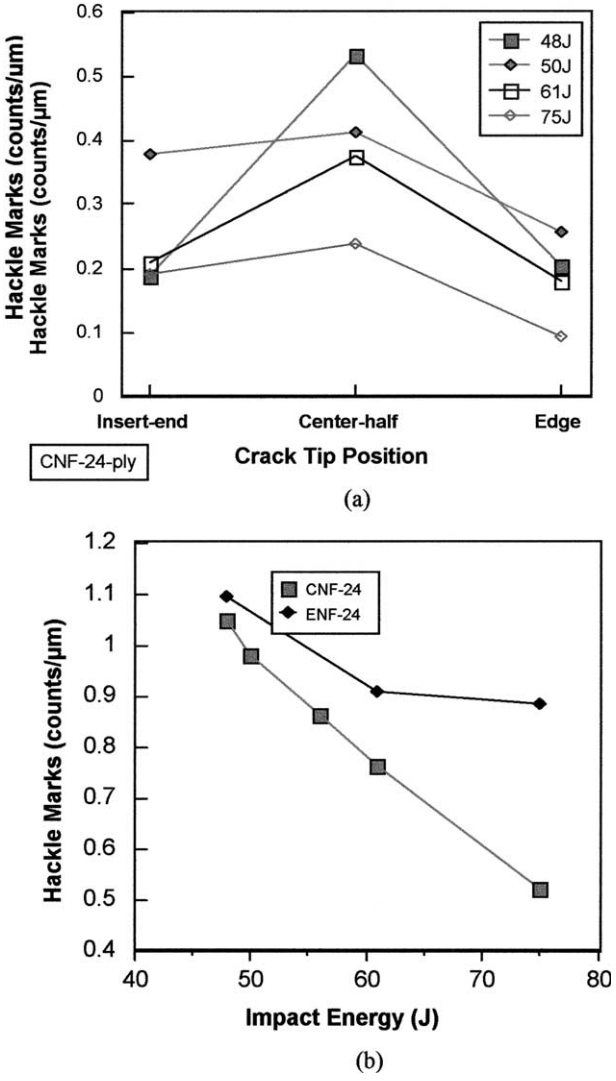

Fig. 11. Variation of hackle marks with loading energy for 24-ply ENF and CNF fracture surfaces.

4.6. Discussions

Complete understanding of these SEM images with reference to the mechanism of fracture at the atomic level is a challenge. The presence and distribution of these hackles show very interesting phenomena at an atomic level, and lead one to the question as to why and how the growth of a crack actually produces the observed atomic phenomena. In brittle materials with an initial crack, it is conceivable that the tip of this crack will decrease or sharpen down to an atomic dimension of the material. The largest stress to tear a crack in tension acts strongly ahead of the crack tip but at right angles to the direction of motion. Marder and Fineberg [40] showed that cracks in brittle materials suffer a dynamic instability going through some distinct stages of propagation. The motion of the crack is forbidden at certain ranges of velocities. Close to threshold crack initiation velocity, the crack velocity is smooth, and increases very slowly, and the motion of the crack is stable. This leaves new and smooth surfaces behind. The motion becomes unstable and surfaces become rougher when the velocity is much higher than the initial threshold velocity. This explains why the hackles are found more at the insert point than as the crack tip approaches the edge. Since the crack is initiated at the insert point, the crack velocity is stable at that point. Thus, uniform distribution of hackle marks is expected at the point of stable velocity and delamination. Once the instability has started, higher energy only results in the creation of more rough surface damage instead of greater propagation. This also supports the results in this study that show a decrease in hackles formation as the energy is increased.

Although the dynamic fracture behavior reported in this investigation agrees with previous quasi-static behavior [24, 25], the values of the energy release rate obtained using the stress-field peak loading force, P_m, differ from the value

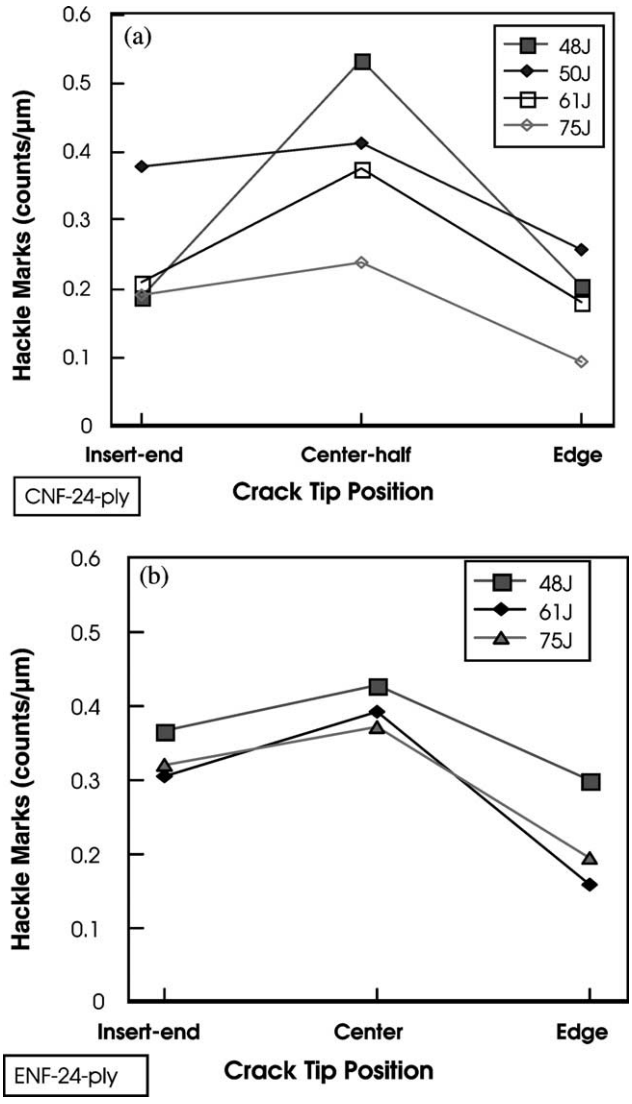

Fig. 12. Variation of hackle marks density with position of crack tip for 24 ply (a) CNF and (b) ENF specimens dynamically loaded at varying energies.

determined conventionally using critical load, P_c, taken at the point where the load–displacement curve deviates from a linear response. It is important to note that P_m is the critical force at which the specimen begins to unload itself (in tension) of the initial compressive stress field. Thus, its use represents the real time stress condition at the crack tip. For static and quasi-static cases, P_c can be known exactly. Since a typical stress-field depended P_m value is more than 10 times higher than P_c, the resulting energy release rate may differ by a factor of more than 100. Thus, the use of P_c may underestimate the energy release rate at high strain rate conditions. In a recent paper by Tsai et al. [31] using modified ENF loaded with MTS, it was observed that the dynamic fracture toughness was the same as the static fracture toughness up to the crack speed of 1100 m/s. Some investigators [41] reported an increase with crack speed while others [42] reported a decrease at certain speeds. These apparent inconsistencies are due to the lack of actual knowledge of the true stress field at the crack tip. Since the loading force P_m is proportional to the amplitude of the stress field, an investigation of the true stress condition at the crack tip using embedded optical fiber sensor is the subject of ongoing investigation. However, the results in this paper do point to the fact that dynamic fracture phenomena are controlled mainly by the magnitude of the stress fields around the crack front. Such stress is needed to determine the true value of the loading force.

5. Conclusions

A power law empirical model reasonably described the variation of the energy release rate with delamination, energy absorbed, and impact energy. Delamination increases with impact energy up to a certain maximum depending on mode of fracture, with CNF > ENF. Dynamic fracture produces fragmentation that depends on the strain rate and energy. CNF pure mode II failure mode at symmetric loading ($D = 0$) causes more fragmentation than ENF. Delamination and energy absorbed in fracture increases with impact energy. Hackle density in mode II fracture surfaces decrease as the delamination length approaches the span of the specimen or as the energy approaches the critical energy for unstable delamination. A crack embedded deeper in a specimen (as in CNF pure mode II) contributes more to mode II fracture than cracks at the surface or near the edge as in ENF. The CNF specimens exhibit a higher compressive strength and sustain higher energy absorption than the ENF. This implies that a crack near the surface or edge of a structure will have a greater tendency to reduce the strength of the materials to failure than when embedded deeper in the structure.

Acknowledgements

This research work was supported by Flight Dynamics Directorate, Wright Laboratory, Wright Patterson Air Force Base, Ohio. Dr Arnold Mayer was the technical monitor.

References

[1] Zukas JA, Nicholas T, Swift HF, Greszczuk LB, Curran DR. Impact dynamics. Florida: Krieger Publishing Company; 1992.
[2] Meyers MA. Dynamic behavior of materials. New York: Wiley; 1994.
[3] Rosakis AJ, Ravichandran G. Dynamic failure behavior. Int J Solids Struct 2000;37:331–48.
[4] Abraham F. The atomic dynamics of fracture. J Mech Phys Solids 2001;49:2095–111.
[5] Oleaga G. Remarks on the basic laws for dynamic crack propagation. J Mech Phys Solids 2001;49:2273–306.
[6] Zou Z, Reid SR, Soden PD, Li S. Mode separation of energy release rate for delamination in composite laminates using sublaminates. Int J Solids Struct 2001;38:2597–613.
[7] Freund LB. Dynamic fracture mechanics. Cambridge: Cambridge Press; 1990.

[8] Joshi SP, Sun CT. Impact induced fracture initiation, and detailed dynamic stress field in the vicinity of the impact. Proceedings of the American Society for Composites, Second Technical Conference, Dearborn; September 1987. p. 117–85.
[9] Liu D. Impact-induced delamination—a view of bending stiffness mismatching. Proceedings of 36th AIAA Structures, Structural Dynamics and Materials Conference; July 1988. p. 674–92.
[10] Foos BC. Damage progression in composite plates due to low velocity impact. Thesis. Department of Civil Engineering, Ohio State University; 1990.
[11] Hopkinson B. A method of measuring the pressure produced in the detonation of high explosives or by the impact of bullets. Phil Trans Roy Soc, Lond, Ser A 1914;213(10):437–56.
[12] Kolsky H. Stress waves in solids. Oxford: Clarendon Press; 1963.
[13] Jahsman WE. Reexamination of the Kolsky techniques for measuring dynamic materials behavior. J Appl Mech 1971;38:77–82.
[14] Zhao H, Gary G. On the use of SHPB techniques to determine the dynamic behavior of materials in the range of small strain. Int J Solids Struct 1996;33(23):3363–77.
[15] Follansbee PS, Frantz C. Wave propagation in the split Hopkinson pressure bar. J Engng Mater Technol 1983;105:61–6.
[16] Gong JC, Malvin LE, Jenkins DA. Dispersion investigation in the split Hopkinson pressure bar. J Engng Mater Technol 1990;112:309–14.
[17] Graaf K. Wave motion in elastic solids. Ohio: Ohio State University Press; 1975.
[18] Bertholf LD. Feasibility of two-dimensional analysis of the split Hopkinson pressure bar system. J Appl Mech 1974;41:137–44.
[19] Lifshitz JM, Leber H. Data processing in the split Hopkinson pressure bar tests. Int J Impact Engng 1994;15(6):723–33.
[20] Dutta PK. The determination of stress waveforms produced by percussive drill pistons of various geometric design. Int J Rock Mech Min Sci 1968;5:501–18.
[21] Bickle LW. An introduction of the use of strain gages for the measurement of propagating strain wave. Sandia Laboratories Report, Albuquerque, New Mexico; 1970.
[22] Ravichandran G, Subbash G. Critical appraisal of limiting strain rates for compression testing of ceramics in a split Hopkinson pressure bar. J Am Ceram Soc 1994;77(1):263–7.
[23] Nwosu SN. High strain rate perforation and mixed mode delamination of laminated composite. Wright laboratory, Final Report; 1977.
[24] Reeder J. Bilinear failure criterion for mixed mode delamination, composite materials: testing and design 11. Philadelphia: ASTM; 1993. p. 303–22.
[25] Reeder JR, Crews JH. Redesign of mixed mode bending test to reduce nonlinear effects. JCTRER 1992;14(1):12–19.
[26] Kazzmarek K. Determination of delamination onset in composite laminates by application of acoustic emission. Proceedings of ICCM-12, Paris; July 1999, paper no. 1223.
[27] Hu N, Fukunaga H. Delamination identification using piezoelectric sensors. In: Proceedings of ICCM-13, Beijing. Paper 1308 June 2001:1010.
[28] Schultz MJ, Pai PF, Inman DJ. Health monitoring and active control of composite structure using piezoelectric patches. Compos, Part B 1999;30(7):713–25.
[29] Penn LS, Jump JR, Greenfield MT, Blanford GE. Use of the free vibration spectrum to detect delamination in thick composite. J Compos Mater 1999;33(1):54–72.
[30] Nakamura T, Kushner A, Lo CY. Interlaminar dynamic crack propagation. Int J Solids Struct 1995;32(17/18):3657–75.
[31] Tsai JL, Guo C, Sun CT. Dynamic delamination fracture toughness in unidirectional polymeric composites. Compos Sci Technol 2001; 61(1):87–94.
[32] Hashemi S, Kinlogh AK, Williams JG. The analysis of interlaminar fracture in uniaxial fiber–polymer composites. Proceedings of Royal Society, London, vol. A427; 1990. p. 173–99.
[33] Williams JG. On the calculation of energy release rate for cracked laminates. Int J Fract 1988;36:101–19.
[34] O'Brien TK, Martin RH. Round robin testing for mode I interlaminar fracture toughness of composite materials. J Compos Technol Res 1993;15(4):269–81. Standard test method for mode I mode I interlaminar fracture toughness of unidirectional fiber-reinforced polymer matrix composites in ASTM Annual Book of Standards, 15.03, 272–80.
[35] Wnag Y, Williams JG. Correction factors for mode II interlaminar toughness tests (ELS and ELF). Proceedings of the Eighth International Conference on Composite Materials, ICCM-8, Honolulu; 1991.
[36] Sriram P, Khourchid Y, Hooper SJ, Martin RH. Experimental development of mixed-mode fatigue delamination criterion. Composite materials: testing and design 5. ASTM.
[37] Sriram P, Khourchid Y, Hooper SJ, Martin RH. Experimental development of mixed-mode fatigue delamination criterion. Composite materials: testing and design 5. ASTM STP 1230, Philadelphia: ASTM; 1995. p. 3–18.
[38] Nwosu SN, Hui D, Czarnecki G. Mode II and mixed mode I/II delamination of graphite/epoxy composite under dynamic loading conditions. Proceedings of ICCM/12 Conference, Paris; July 1999, paper 1363.
[39] Nwosu SN, Hui D. Characterization of dynamic fracture mode of composite materials by hackle marks linear density. Proceedings of ICCM/13 Conference, Beijing; June 2001, paper 1663.
[40] Marder M, Fineberg J. How things break. Phys Today 1996; September:24–9.
[41] Aliyu AA, Daniel IM. Effect of strain rate on delamination fracture toughness of graphite/epoxy. In: Johnson WS, editor. Delamination and debonding of materials. ASTM STP 876, Philadelphia: ASTM; 1985. p. 336–48.
[42] Yaniv G, Daniel IM. Height-tapered double cantilever beam specimen for study of rate effects on fracture toughness of composites. In: Whitecomb JD, editor. Composite materials: testing and design. ASTM STP 972, Philadelphia: ASTM; 1988. p. 241–58.